A topographic drag closure with analytically derived base flux

by

Stephen T. Garner
Geophysical Fluid Dynamics Laboratory/NOAA
Princeton NJ

June 2003

Abstract

Recent improvements in closure schemes for topographic drag in large-scale models have focused on better characterizations of the mean height, scale, orientation and anisotropy of the subgrid topography. However, under certain assumptions, linear analysis provides the exact amplitude and orientation of the drag without relying on statistical properties of the terrain. The author proposes a computationally practical analytical closure based on the known subgrid topography. A nonlinear correction patterned after existing schemes for nonpropagating base flux is also proposed. The novelty of this correction is to exploit information about the range of mountain heights within grid cells. When the correction is interpreted as a formula for the transition to saturation, it also provides a way of estimating the vertical distribution of the momentum forcing.

1. Introduction

Mountain drag parameterization schemes come in two parts. The first provides the total source or sink of momentum at the ground (the "base flux") and the second specifies the vertical distribution of forcing by estimating how the wave train deposits the momentum perturbation. Previous schemes for estimating the base flux rely on statistical measures of the height, shape and orientation of the unresolved terrain (e.g., Baines and Palmer 1990, Lott and Miller 1997, Scinocca and McFarlane 2000). Here we propose an analytical estimate of the drag vector. This base-flux estimate is exact if the mountain waves are linear and hydrostatic and if the medium is nonrotating and uniform in time and space.

We also propose a straightforward correction for nonlinearity at the source. This correction is guided by older schemes that allow a gradual transition between linear and nonlinear dimensional drag laws (*e.g.*, Pierrehumbert 1987, Lott and Miller 1997). However, in the proposed treatment, the transition is based on the known range of mountain heights within the grid cell. Reference to these subgrid topographic heights also leads to a refinement of the rule for clipping the wave amplitude to the saturation value as a function of height. The new closure scheme has the concrete advantage of removing two of the free parameters appearing in traditional schemes for mountain wave drag.

2. Base-flux closure

Nearly all parameterizations for radiating mountain waves assume steady, linear, upward-propagating gravity waves. If we add to these assumptions certain constraints on the horizontal scale of the forcing, such that the waves are broad enough to be hydrostatic but narrow enough to be unaffected by sphericity, rotation or the ambient baroclinicity, we can calculate the total source as accurately as we know the shape of the terrain. This accuracy will not extend to the correction for nonlinearity at the source or to the evaluation of the momentum forcing due to breaking.

2a. Linear part

We suppose that the topography can be analyzed into Fourier amplitudes $\tilde{h}(\boldsymbol{k})$, where $\boldsymbol{k} = (k, l)$ is the horizontal wavenumber. This is a reasonable starting place because the scales of interest are much smaller than the planetary scale. We write $\overline{V}_{\perp\boldsymbol{k}} \equiv \overline{\boldsymbol{V}} \cdot \boldsymbol{k}/|\boldsymbol{k}|$ for the component of the large-scale flow, $\overline{\boldsymbol{V}}$, along the gradient of the terrain component with wavenumber $\boldsymbol{k}$. Then the linearized boundary condition is

$$\tilde{W}(\boldsymbol{k}) = \overline{V}_{\perp\boldsymbol{k}} i|\boldsymbol{k}|\tilde{h}(\boldsymbol{k}), \tag{1}$$

where $\tilde{W}$ is the transform of $W(x, y) \equiv w(x, y, z = 0)$, the vertical velocity component at the surface. With this transform, we have also assumed that the mountain waves have much smaller horizontal scales than all other types of variability in the flow.

We neglect temporal variations of $\overline{\boldsymbol{V}}$ and assume gradual vertical variations such that $d(|m|^{-1})/dz \ll 1$, where m is the stationary vertical wavenumber. If we also ignore horizontal variations of the buoyancy frequency, $\overline{N}$, and consider only hydrostatic scales $|k| \ll m$, the WKB approximation for the vertical structure is

$$\tilde{w}(\boldsymbol{k}, z) = \tilde{W}(\boldsymbol{k})\exp\left(i\int_0^z m dz'\right), \tag{2}$$

with $m \approx \overline{N}/\overline{V}_{\perp\boldsymbol{k}}$. It then follows from (1) and (2) that, at the surface,

$$\partial\tilde{w}/dz = -\overline{N}|\boldsymbol{k}|\tilde{h}. \tag{3}$$

The derivative is independent of $\overline{V}_{\perp\boldsymbol{k}}$, as is the horizontal velocity perturbation associated with *w*. This velocity, say $\boldsymbol{V}'$, is completely determined by a velocity potential, $\chi(x, y)$, such that $\nabla\chi = \boldsymbol{V}'$. If we neglect density variations, conservation of mass implies $\nabla^2\chi = -\partial w/dz$.

Then, using (3), we have $\tilde{\chi}(\boldsymbol{k}) = -(\bar{N}/|\boldsymbol{k}|)\tilde{h}(\boldsymbol{k})$. The synthesis is

$$\chi(x, y) = -\bar{N}\iint\frac{\tilde{h}(\boldsymbol{k})}{|\boldsymbol{k}|}\exp(i\boldsymbol{k}\cdot\boldsymbol{x})dkdl\,, \tag{4}$$

where $\boldsymbol{x} = (x, y)$. Thus, χ is a slightly smoothed transformation of the terrain height. The spatial-transform equivalent of (4) is

$$\boxed{\chi(x, y) = -\frac{\bar{N}}{2\pi}\iint\frac{h(\boldsymbol{x}')}{|\boldsymbol{x}-\boldsymbol{x}'|}dx'dy'}\,. \tag{5}$$

The velocity perturbation $\nabla\chi$ produced by each spectral component of $h(x, y)$ is perpendicular to the corresponding phase lines of the topography and directed downhill. For physical consistency, it is necessary to filter the input topography so as to retain only the scales that force stationary gravity waves. We will return to this problem later.

The subgrid velocity perturbation $\nabla\chi \equiv \boldsymbol{V}'$ is independent of the resolved velocity $\bar{\boldsymbol{V}}(x, y)$. However, the momentum flux across a horizontal surface, namely,

$$\tau(x, y) = \bar{\rho}w\boldsymbol{V}'\,, \tag{6}$$

depends on the resolved wind through $w = \bar{\boldsymbol{V}}\cdot\nabla h$. Let $\chi_0 = (N_0/\bar{N})\chi$, where N_0 is a constant buoyancy frequency. Then

$$\tau = \frac{\bar{\rho}\bar{N}}{\rho_0 N_0}[\rho_0\nabla\chi_0(\nabla h)^T]\bar{\boldsymbol{V}}\,. \tag{7}$$

The quantity in brackets, $\rho_0\nabla\chi_0(\nabla h)^T \equiv \mathbf{T}$, is an outer product of two-dimensional vectors that depend only on the terrain. Subject to our assumptions, it contains all relevant information about the topography, including amplitude, variance and anisotropy. Using angle brackets to denote a grid-cell average, we can write

$$\boxed{\langle \tau \rangle \;=\; \frac{\bar{\rho}\bar{N}}{\rho_0 N_0} \langle \mathbf{T} \rangle \bar{\boldsymbol{V}}} \tag{8}$$

for the estimate of drag at a model grid-point. In spectral models, it should be consistent to regard (4) as an integral over spherical harmonics by interpreting $|\boldsymbol{k}|$ as the total spherical-harmonic wavenumber l, since planetary scales are not directly involved.

In the examples to follow, we obtain the mountain-wave disturbance from (5) using distances measured on a spherical surface. To remove the large scales, we pre-process the topography using a filter that passes only scales of less than about 1.5 degrees of longitude and latitude in the extratropics. This filtering scale, d, is allowed to vary with latitude so as to keep the Rossby number V/fd of order unity, where $V(y)$ is a profile of typical surface wind speeds and $f(y)$ is the Coriolis parameter. The horizontal derivatives in (8) make the result rather insensitive to the choice of scales retained by a high-pass filter, and this allows a time-independent choice for $d(y)$. In a departure from earlier schemes, we propose to make the filter independent of model resolution. We do this by defining "subgrid drag" to be the difference between the parameterized drag and the model's resolved drag. In most climate-model applications, the resolved drag can be treated as zero; otherwise, the resolved base flux has to be diagnosed at each time step.

From (5), note that the velocity scales as $N_0 h_0$, where h_0 is a measure of the mesoscale component of the topographic height. Therefore, mountain-wave velocities have an order of magnitude of $V' \sim (10^{-2}\mathrm{s}^{-1})(10^3\mathrm{m}) \;=\; 10\mathrm{ms}^{-1}$, given a typical mesoscale relief of $1000\ \mathrm{m}$. If the horizontal scale of these features is 100 km and the large-scale wind is also of order 10 ms^{-1}, the vertical velocity is of order 0.1 ms^{-1}, and it follows that the drag is characteristically $D \sim \rho_0(10\mathrm{ms}^{-1})(0.1\mathrm{ms}^{-1}) \sim 1\mathrm{Pa}$. The tensor $\mathbf{T}$ is dominated by the diagonal elements, which are of the order of $\rho_0(10\mathrm{ms}^{-1})$.

Shown in Fig. 1 is a plot of the linear drag $\langle\tau\rangle$ over the Western Hemisphere. The assumed large-scale wind is purely zonal at -8 m/s in the tropics and 13 m/s in the extratropics. A constant buoyancy frequency, $N_0 = 0.01\,\mathrm{s}^{-1}$, is assumed. Fig. 2 is the same as Fig. 1 but for the Asian continent and for an assumed large-scale wind from the west at 10 m/s everywhere. The averaging in both Fig. 1 and Fig. 2 is over latitude-longitude cells of about 1.5 degrees on a side. The topographic data have a resolution of 1/30 degree.

2b. Nonlinear part

There are three nonlinearities determining the stationary disturbance due to mountains. Compared to the linear effects, they are of the order of the nondimensional mountain height, $\mathrm{Fr} = (\bar{N}/\bar{V})h$, and are associated with the first three terms on the right-hand side of the lower boundary condition, written as:

$$w - \bar{\boldsymbol{V}} \cdot \nabla h = \boldsymbol{V}' \cdot \nabla h - \bar{\boldsymbol{V}} \cdot \nabla(\delta_z h) + h\bar{\boldsymbol{V}}_z \cdot \nabla h + \ldots \tag{9}$$

In this perturbation series, δ is the lowest-order vertical particle displacement (with δ_z its first derivative) and $\bar{\boldsymbol{V}}_z$ is the resolved shear.

The first two nonlinear terms in (9) are associated with low-level blocking (e.g., Pierrehumbert and Wyman 1985), deflection (*e.g.*, Miranda and James 1992) and periodic “steepening” above the mountain (*e.g.*, Smith 1977). These processes alter the total drag and cause some of it to be deposited at low levels close to the source. Let us refer to this part of the base flux as “non-propagating”. The remaining term on the right-hand side of (9) could be included analytically by replacing (8) with

$$\langle\tau\rangle = \frac{\bar{\rho}\bar{N}}{\rho_0 N_0}(\langle\mathbf{T}\rangle\bar{\boldsymbol{V}} + \langle\mathbf{S}\rangle\bar{\boldsymbol{V}}_z), \tag{10}$$

where $\mathbf{S} = \rho_0 h \nabla\chi_0 (\nabla h)^T$. However, this correction is less significant than the other two nonlinear effects when the local Richardson number, $\bar{N}^2/(\bar{\boldsymbol{V}}_z)^2$, is large. The Richardson number is assumed to be large in making the WKB approximation leading to (4). Moreover, the uncertainty about the proper value of $\bar{\boldsymbol{V}}$ to use in the presence of a planetary mixed layer could easily exceed the size of any correction due to $\bar{\boldsymbol{V}}_z$.

We propose to evaluate the nonpropagating drag associated with "tall" mountains by using a dimensional analysis and assuming an "orographic adjustment" process (Pierrehumbert and Wyman 1985, Pierrehumbert 1987). What follows is a fairly standard treatment along these lines (*e.g.*, Lott and Miller 1997), except that we will allow for a range of mountain heights within the grid cell. The nonlinear correction will be treated as much as possible as an extension of the linear result, in order to take advantage of the good dynamical information in that part of the scheme. In particular, we will assume that the transition to nonlinear flow preserves the direction of the net drag within the grid cell.

Since "excess" mountain height cannot be straightforwardly attributed to spectral components, we assume that the topography is characterized by well-defined features that can be binned into height ranges with well-defined areal coverage. If the mountain height exceeds a certain order-unity threshold, h_c that depends on both $\bar{V}$ and $\bar{N}$, the flow is blocked or deflected below a level $z = h - h_c$. For terrain features with heights less than h_c, the drag is entirely linear and propagating. For those greater than h_c, it includes a propagating and a nonpropagating contribution, as shown schematically in Fig. 3. The part that launches internal waves has a height of h_c measuring down from the summit. A power law with parameter β is introduced in order to relate

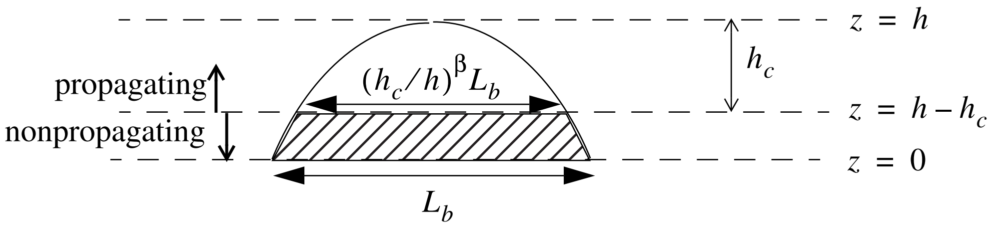

Fig. 3

the width L of this part of the mountain to elevation above the base: $L(z) = L_b(1 - z/h)^{\beta}$. Thus, $\beta = 1$ corresponds to triangular mountains, $\beta < 1$ to blunt mountains and $\beta > 1$ to pointed ones.

As the flow becomes blocked by topography, the drag law in the blocked layer changes from $D \sim \rho N V h^2 / L$ to $D \sim \rho V^2 (h - h_c)/L$, where V and L are the ambient wind component and length of the mountain, respectively, in the direction of the drag. The assumption of orographic adjustment essentially means that the nondimenisonal depth $\tilde{h} = h(\bar{N}/\bar{V})$ of the unblocked flow below the summit is set by a universal threshold, $\tilde{h}_c = h_c(\bar{N}/\bar{V})$, related to the critical Froude number.

Combining these assumptions, we find that the drag is:

$$\begin{aligned} D_p &= a_0 \min\{1, (\tilde{h}_c/\tilde{h})^{2-\beta}\} \tilde{h}^2 (\bar{\rho}\bar{V}^3/\bar{N}L_b), \\ D_{np} &= a_1(1 - \min\{1, (\tilde{h}_c/\tilde{h})^{1+\beta}\}) \frac{\tilde{h}}{1+\beta} (\bar{\rho}\bar{V}^3/\bar{N}L_b), \end{aligned} \tag{11}$$

where D_p and D_{np} refer to the vertically propagating and nonpropagating parts of the base flux, respectively, and a_0 and a_1 are constants. This purely dimensional formulation is similar to that of Lott and Miller (1997), but it uses the additional parameter β and limits the propagating drag to a residual when $\mathrm{Fr} > \mathrm{Fr}_c$. The parameter β also appears in D_{np}. This is because the vertical cross-section of the obstacle within the blocked layer -- shown hatched in Fig. 3 -- is reduced by the tapering of the mountain when $\beta > 0$.

To integrate (11) over the grid cell, we need a relationship between h and L_b. It is impractical to use the detailed subgrid height distribution because while $\tilde{h}_c$ is assumed constant, $\tilde{h}$ is time-dependent. The analysis in the appendix suggests that for heights exceeding a certain threshold of around 200 m, we may assume a power law,

$$L/L_0 = (h/h_0)^{\gamma}, \tag{12}$$

where L_0, h_0 and γ are universal constants. This seems to suggest a $-2/\gamma$ power spectrum for topographic height, but (12) actually approximates a probability distribution function across *bins* rather than spectral components. If we can neglect overlaps between terrain features and ignore any correlation between anisotropy and mountain height, the areal coverage $dA \sim LdL$ of features in the range from $\tilde{h}$ to $\tilde{h} + d\tilde{h}$ will be proportional to $n(\tilde{h})\tilde{h}^{2\gamma-1}d\tilde{h}$, where $n(\tilde{h})$ is the number of features in the range. For this number we assume another power law, namely, $n(h) = n_0(h/h_1)^{-\varepsilon}$. The constants n_0 and h_1 will not appear in any results, but are constrained by the assumption of nonoverlapping features and by the area of the grid cell.

If we take $\overline{V}$ and $\overline{N}$ constant over the grid cell and use the stated assumptions about the mountain height distribution, we can integrate (11) with respect to area to obtain

$$\begin{aligned}
\langle D_p \rangle &= a_0 \tilde{h}_0^{\gamma} \frac{H^{<}(\gamma - \varepsilon + 2) + H^{>}(\gamma - \varepsilon - \beta)}{H(2\gamma - \varepsilon)} (\bar{\rho}\overline{V}^3/\overline{N}L_0) \\
\langle D_{np} \rangle &= a_1 \tilde{h}_0^{\gamma} \frac{H^{>}(\gamma - \varepsilon + 1) - H^{>}(\gamma - \varepsilon - \beta)}{(1+\beta)H(2\gamma - \varepsilon)} (\bar{\rho}\overline{V}^3/\overline{N}L_0)
\end{aligned} \tag{13}$$

for the average drag. Here $H(\alpha) \equiv [(\tilde{h}_{max})^{\alpha} - (\tilde{h}_{min})^{\alpha}]/\alpha$, and the superscript on H means that $\tilde{h}$ is replaced with either $\tilde{h}^{<} \equiv \min(\tilde{h}, \tilde{h}_c)$ or $\tilde{h}^{>} \equiv \max(\tilde{h}, \tilde{h}_c)$. Note that $H(0) = \log(\tilde{h}_{max}/\tilde{h}_{min})$. The result for D_p includes the effect of reducing the forcing area element dA by the factor $(\tilde{h}/\tilde{h}_c)^{-2\beta}$, as implied in Fig. 3. This is a horizontal "clipping" somewhat similar to that described by Lindzen (1988).

For h_{min} and h_{max}, one could use the actual minimum and maximum from the set of local extrema of high-pass topography within the cell. However, there is a great deal of scatter in the actual L-h relationship, as discussed in the appendix. We prefer a less erratic estimate of these height limits. We find that $h_{min} \ll h_{max}$ holds quite universally. Therefore we propose to equate $\langle D_p \rangle$ in (13) to the actual average of D_p in (11) over each grid cell, using the small-amplitude ($\tilde{h} \to 0$) limit in both equations. This yields the desired distribution of h_{max} if we assume $h_{min} = \mu h_{max}$ for some fixed μ. In the small-amplitude limit, (13) reduces to $\langle D \rangle = D^*$, where

$$D^* \equiv a_0 \bar{\rho} \bar{N} \bar{V} \eta^2 / L_0 \tag{14}$$

and

$$\eta \equiv \tilde{h}_0^{\gamma/2} \frac{\bar{V}}{\bar{\bar{N}}} \left(\frac{H(\gamma - \varepsilon + 2)}{H(2\gamma - \varepsilon)} \right)^{1/2} . \tag{15}$$

Ttraditional schemes for linear base flux generally use (14) with η identified as the root-mean-squared height of the filtered topography.

In Fig. 4, we show the linear base flux due to a uniform westerly wind over Europe and Asia computed in three different ways. The first (“drag1”) is obtained from (8) in the scalar form

$$D = \bar{\rho} \frac{\bar{V}}{2} \mathrm{Tr}(\mathbf{T}), \tag{16}$$

while the second and third are computed from (14). The second computation (“drag2”) uses the filtered topographic variance $\eta^2 = \langle h^2 \rangle$ and the third (“drag3”) uses the formula (15) for η, with $h_{min} = 0$ (or $\mu = 0$). The dimensional expression with $\eta^2 = \langle h^2 \rangle$ has been tuned to provide a good match to the analytic result over the highest terrain, but it then misses many of the lower features. By contrast, the dimensional analysis using (15) matches the analytic base flux almost everywhere within a factor of two (this holds over the earth’s entire land surface). The “best-match” parameters used in this result are $a_0 = 2$ (for both drag2 and drag3), $\tilde{h}_0 = 1$,

$\gamma = 0.4$ and $\varepsilon = 0$.

Clearly (10) is a better linear drag formula than (14). Our only purpose in introducing the latter is to partition the drag between propagating and nonpropagating components. In effect, we determine a_0 as a function of latitude and longitude by setting $|\langle\tau\rangle| = \langle D\rangle$ and then substituting $\langle\tau\rangle = \tau^*$ evaluated from (8) and $\langle D\rangle = D^*$ evaluated from (14). As noted above, a_0 ranges roughly between 1 and 4 over the earth's land surface. We use this result in (12), allowing (10) to determine the direction of the drag. Thus, the base flux, as modified by the bulk dimensional analysis, is

$$\langle\tau\rangle = \left(\frac{\langle D_p\rangle}{D^*} + \frac{\langle D_{np}\rangle}{D^*}\right)\tau^*. \tag{17}$$

The nonpropagating part should be applied to the resolved momentum below a reference level while the propagating part should be distributed over the column according to a level-by-level determination of wave saturation.

The transition from linear flux to saturation flux for the two extreme cases of $\tilde{h}_{min}/\tilde{h}_{max}$ is shown in Fig. 5, in which $\langle D_p\rangle/D^*$ is graphed as a function of $\tilde{h}_{max}/\tilde{h}_c$ with $\gamma = 0.4$, $\beta = 0.5$ and $\varepsilon = 0.2$. Also shown is the total normalized drag $(\langle D_p\rangle + \langle D_{np}\rangle)/D^*$ based on the additional assumption that $a_1/a_0 = 9.0\tilde{h}_c$. This choice for a_1 produces a maximum total drag of approximately $2D^*$, which is a compromise between the maximum drags obtained in two- and three-dimensional nonlinear simulations, as summarized by Lott and Miller (1997) and Scinocca and McFarlane (2000). The sharpest transitions in both D_p and D_{np} occur for $\tilde{h}_{max} \approx \tilde{h}_{min}$. Results are less sensitive to γ, but large values of this parameter make the transitions sharper (not shown).

Shown in Fig. 6 is the normalized propagating and nonpropagating bulk-dimensional drag for North America based on the same parameter choices as in Fig. 5. The assumed large-scale wind, needed for determining the range of $\tilde{h}$, is purely zonal at 8 m/s in the extratropics and -5 m/s in the tropics, and the static stability is taken to be $\overline{N} = 0.01\ \mathrm{s}^{-1}$ everywhere. With these choices, we find that the flow over the Rocky Mountains is significantly nonlinear at all latitudes.

3. Level-by-level determination of momentum forcing

To obtain the momentum forcing from $\partial\overline{\mathbf{V}}/\partial t = \ldots - \bar{\rho}^{-1} d\langle\tau\rangle/dz$, we need the vertical profile $\langle\tau(z)\rangle$. Let $\delta(z)$ denote the vertical particle displacement in a stationary mountain wave and define $\tilde{h}(z) = \overline{N}\delta/\overline{V}$, where $\overline{N}(z)$ is the buoyancy frequency and $\overline{V}(z)$ is the resolved wind component in the direction opposite the net drag. We also assume a density profile $\bar{\rho}(z)$. By defining $U(\tilde{h}, z) = \tilde{h}\sqrt{(\bar{\rho}/\rho_0)\overline{V}^3/\overline{N}L} = h\sqrt{(\bar{\rho}/\rho_0)\overline{N}\overline{V}/L}$, a function of both the mountain amplitude and the environment at height z, we can write the integral of the propagating part of (11) as

$$\langle D_p(0)\rangle = a_0 \frac{(2\gamma' + \varepsilon)U_0^{\gamma'+\varepsilon}}{U_{max}^{2\gamma'+\varepsilon} - U_{min}^{2\gamma'+\varepsilon}} \rho_0 \left(\frac{\hat{U}_c^{\gamma'+2} - U_{min}^{\gamma'+2}}{\gamma'+2} + \frac{U_{max}^{\gamma'-\beta} - \hat{U}_c^{\gamma'-\beta}}{\gamma'-\beta} U_c^{\beta} U_c^2 \right), \tag{18}$$

where $\gamma' = \gamma - \varepsilon$ and $\hat{U}_c \equiv \min[U_{max}, \max(U_{min}, U_c)]$. The quantity $\rho_0 U^2$ is proportional to the areally averaged vertical momentum flux. Therefore, according to the theorem of Eliassen and Palm (1960), the value of U associated with a particular feature is independent of z until that part of the disturbance breaks. We are able to retain this constraint after wavebreaking because the saturated drag does not depend on h. In the end, the integration of the drag with respect to the terrain always ranges over the same interval, U_{min} to U_{max}.

If we assume that the horizontal scales of the individual features do not change as a result of wavebreaking over the source, the average flux as a function of height can be written

$$\boxed{\langle D_p(z)\rangle = a_0 \frac{(2\gamma' + \varepsilon)U_0(0)^{\gamma'+\varepsilon}}{U_{max}^{2\gamma'+\varepsilon} - U_{min}^{2\gamma'+\varepsilon}} \rho_0[R_u(z) + R_b(z)] ,} \tag{19}$$

where $U_0(z) = U(h_0, z)$ and the flux has been partitioned into unbroken and broken components, R_u and R_b, respectively, corresponding to the two terms in parentheses in (18). Let $V_c(z) = \min|_{z' < z}\{U_c(z')\}$. Then

$$R_u = \frac{\hat{V}_c^{\gamma'+2} - U_{min}^{\gamma'+2}}{\gamma' + 2}$$
$$R_b = \left(\frac{\hat{U}_c(0)^{\gamma'} - \hat{V}_c^{\gamma'}}{\gamma'} + \frac{U_{max}^{\gamma'-\beta} - \hat{U}_c(0)^{\gamma'-\beta}}{\gamma' - \beta} U_c(0)^{\beta}\right) V_c^2 , \tag{20}$$

where $\hat{V}_c \equiv \min[U_{max}, \max(U_{min}, V_c)]$. This “saturation profile” specifies how the momentum flux associated with the full range of terrain features is limited by the local saturation flux, proportional to $D_{sat} \equiv \rho_0 U_c^2$. We have assumed in (19) that the disturbance cannot gain energy from the environment. This means that the residual flux from the broken components, proportional to $\rho_0 V_c^2$, will fall below the local saturation wherever U_c increases with z.

In Fig. 7, we graph $r_p(z) \equiv \langle D_p\rangle / D^*$ to show the transition to saturation as a function of height above the mountains for two different ranges of $\tilde{h}$ and an assumed environmental column described in the caption. The dashed curve is the local saturation value, D_{sat}. Momentum anomaly is deposited in the layers where D_p is decreasing, which, in this case, occur just above the two assumed jets. The waves take longest to fully saturate when the terrain features within grid cells vary most widely in height ($\tilde{h}_{min}/\tilde{h}_{max} = 0$).

The present saturation condition is based on the component of mean wind in the direction of the *aggregate* drag in the grid cell. Neglecting the subgrid variation of drag direction affects not only the base flux but also the vertical flux profile if the ambient wind turns with height. The latter effect was analyzed by Shutts (1995). In the case of real topography, there is no universal relationship between the subgrid drag direction and subgrid mountain height, which would be needed to make a correction to (18). We are also neglecting the possibility of re-radiation from breaking regions (Bacmeister and Schoeberl 1989).

4. Unsteady resolved flow

The steady-state situation that we have analyzed is the limit of very short advective time scales compared to the time scales of the background flow: $\bar{V}|\boldsymbol{k}| \gg \omega_0$ in the case of a single background frequency, ω_0. The opposite limit $\bar{V}|\boldsymbol{k}| \ll \omega_0$ is also easy to analyze (the linear solution in the general case is given by Bell, 1975). In fact, it produces essentially the same drag formula as in the steady case.

Thus, if $\omega_0 \gg \bar{V}|\boldsymbol{k}|$, we can proceed from (2) but with $m = -\bar{N}|k|/\sqrt{\omega_0^2 - f^2}$ for the vertical wavenumber, where f is the (slowly varying) Coriolis parameter. We have excluded nonhydrostatic waves by assuming $\omega_0 \ll \bar{N}$. Then (3) is replaced by

$$\partial\tilde{w}/dz = \left(\frac{\bar{N}|\boldsymbol{k}|}{\sqrt{\omega_0^2 - f^2}}\tilde{h}\boldsymbol{k}\right) \cdot \bar{\boldsymbol{V}}. \tag{21}$$

We still have that $\partial w/\partial z = -\nabla \cdot \boldsymbol{V}'$, and since the momentum equation implies

$$\left(\frac{\partial^2}{\partial t^2} + f^2\right)(-\nabla \cdot \boldsymbol{V}') = \bar{\rho}^{-1}\frac{\partial}{\partial t}\nabla^2 p', \tag{22}$$

we may operate on (21) with the transform equivalent of $\rho\nabla^{-2}(f^2 + \partial^2/\partial t^2)$ to reach

$\tilde{p} = \bar{\rho}(\bar{S}\tilde{h}|\boldsymbol{k}|^{-1}i\boldsymbol{k}) \cdot \overline{\boldsymbol{V}}$, where $\bar{S} \equiv \overline{N}\sqrt{\omega_0^2 - f^2}/\omega_0$. If $\omega_0 > |f|$, the synthesis is

$$p' = -\bar{\rho}\nabla\chi \cdot \overline{\boldsymbol{V}}, \tag{23}$$

where χ is defined by (4) or (5) with $\bar{S}$ replacing $\overline{N}$. In this case, χ is *not* related to the velocity potential for the flow perturbation.

The drag is not due entirely to the eddy momentum flux (in fact, w and V' are in quadrature when $f = 0$), but is still determined by the surface pressure distribution according to

$$\tau = -p'\nabla h = \bar{\rho}[\nabla\chi(\nabla h)^T]\overline{\boldsymbol{V}}. \tag{24}$$

Note that (24) is essentially the same as in the stationary case (7). This result may have applications to small-scale internal waves generated by semi-diurnal tidal flows in the ocean. On the other hand, since the drag is independent of frequency when $\omega_0 \gg f$, (24) is somewhat more general than simple harmonic motion.

In the case of simple harmonic motion, (22) implies that the amplitude of $(\omega_0^2 - f^2)\boldsymbol{V}'(t)$ is the same as that of $\bar{\rho}^{-1}\omega_0\nabla p'(t) = \omega_0\mathbf{A}\overline{\boldsymbol{V}}(t)$, where $A_{ij} = -\frac{\partial}{\partial x_i}\frac{\partial}{\partial x_j}\chi$. The matrix $\mathbf{A}$ is expected to be diagonally dominant with its larger eigenvalue approximated by $\lambda \approx \frac{1}{2}\mathrm{Tr}(\mathbf{A}) = -\frac{1}{2}\nabla^2\chi$. Therefore a reasonable measure of the nonlinarity of the oscillating disturbance is

$$\mathrm{Fr} = |\boldsymbol{V}'|/|\overline{\boldsymbol{V}}| \approx \frac{1}{2}|\nabla^2\chi|\frac{\omega_0}{\omega_0^2 - f^2}. \tag{25}$$

Since $\nabla\chi$ scales as $N_0 h_0$, this result is consistent with Bell (1975) in the limit $\omega_0 \gg |f|$. The velocity perturbation becomes unbounded (resonant) at the latitudes where $\omega_0 = |f|$, but the drag itself vanishes smoothly as these latitudes are approached from the equatorward side.

5. Summary

Linear analysis gives the vector drag due to stationary, hydrostatic, nonrotating waves over topography. Therefore, statistical characterizations of the subgrid terrain are not required for the *linear* base-flux computation. The analytical result leads to a practical closure for numerical general-circulation models. The correction for nonlinearity and the related formula for saturation flux continue to require an *ad-hoc* treatment. We have suggested a dimensional treatment of this part of the forcing that takes advantage of the linear solution. We have also suggested a way to avoid complicated procedures for filtering the topography prior to the determination of the unresolved drag. It turns out that the linear base-flux formula in the case of an unsteady resolved flow is virtually identical to that for a steady background flow if the dominant frequencies satisfy $\omega_0 \gg \bar{V}|\boldsymbol{k}|$ and $\omega_0 > f$.

The base-flux scheme of Pierrehumbert (1987), to take a simple example, is essentially

$$D = G\frac{\tilde{h}^2}{a^2 + \tilde{h}^2}\rho_0 V^3 / NL, \tag{26}$$

in which G and a are fixed parameters. Analogous parameters are needed by more sophisticated schemes, including those of Baines and Palmer (1990), Lott and Miller (1997) and Scinocca and McFarlane (2000). The present approach eliminates the first of the two parameters by providing the amplitude of the linear drag. It also provides the *direction* of the drag. The other parameter, a, is essentially the critical mountain height, but it also determines the ratio of the linear and nonlinear drag coefficients and the rapidity of the transition from linear to nonlinear drag. In the present scheme, the critical mountain height remains a free parameter, $\tilde{h}_c$, as does the nonlinear drag coefficient, a_1. However the functional form of the transition is less arbitrary. This is because (18) incorporates information about the range of mountain heights within each grid cell, subject to the assumed universal power law (12). The abruptness of the transition determines the shallowness of the layer with momentum forcing. The broadening of this layer by the effect of non-parallel vertical shear (Shutts 1995) is missing from the present scheme. However, (13) and (18) do include the effect of horizontal narrowing of the transmitted waves by clipping (e.g., Lindzen 1988), which increases the sensitivity of the forcing layer height and thickness to the range of terrain heights.

The present combination of analytical and dimensional methods for topographic drag closure contrasts with the combination of *statistical* and analytical methods used by Scinocca and McFarlane (2000) and Lott and Miller (1997). The nonpropagating drag estimate is not necessarily better than ones based on a statistical representation of the shape and orientation of the unresolved topography. However, the propagating part of the base flux is almost certainly better estimated by the present method because it is purely analytical and rests on fewer assumptions.

Appendix

We have used for the horizontal scale of a "feature" (a local maximum in that exceed). The scales and can be obtained from the mean values of and . The analysis of high-pass topography presented in the appendix suggests over most parts of the earth's land surface.

References

Bacmeister, J.T., and M.R. Schoeberl, 1989: Breakdown of vertically propagating two-dimensional gravity waves forced by orography. *J. Atmos. Sci.*, **46**, 2109-2134.

Baines, P.G., and T.N. Palmer, 1990: Rationale for a new physically based parametrization of subgridscale orographic effects. Tech. Memo. 169. European Centre for Medium-Range Weather Forecasts.

Bell, T.H., 1975: Lee waves in stratified flows with simple harmonic time dependence. *J. Fluid Mech.*, **67-4**, pp. 705-722.

Eliassen, A., and E. Palm, 1960: On the transfer of energy in stationary mountain waves. *Geofysiske Publikasjoner*, **22**, 1-23.

Lindzen, R.S., 1988: Supersaturation of vertically propagating internal gravity waves. *J. Atmos. Sci.*, **45**, 705-711.

Lott, F., and M.J. Miller, 1997: A new subgrid-scale orographic drag parametrization: Its formulation and testing. *Quart. J. R. Meteor. Soc.*, **123**, 101-127.

Miranda, M.A., and I.N. James, 1992: Non-linear three-dimensional effects on gravity-wave drag: Splitting flow and breaking waves. *Quart. J. R. Meteor. Soc.*, **118**, 1057-1081.

Palmer, T.N., G.J. Shutts, and R. Swinbank, 1986: Alleviation of a systematic westerly bias in general circulation and numerical weather prediction models through an orographic gravity wave drag parameterization. *Quart. J. R. Meteor. Soc.*, **112**, 1001-1039.

Pierrehumbert, R.T, 1987: An essay on the parameterization of orographic gravity wave drag. *Proc. Seminar/Workshop on Observations, Theory and Modeling of Orographic*

Effects,Vol. 1, Shinfield Park, Reading. UK, ECMWF, 251-282.

________________, and B. Wyman, 1985: Upstream effects of mesoscale mountains. *J. Atmos. Sci.*, **42**, 977-1003.

Scinocca, J.F., and N.A. McFarlane, 2000: The parametrization of drag induced by stratified flow over anisotropic orography. *Quart. J. R. Meteor. Soc.*, **126**, 2353-2393.

Shutts, G., 1995: Gravity-wave drag parametrization over complex terrain: The effect of critical-level absorption in directional wind-shear. *Quart. J. R. Meteor. Soc.*, **121**, 1005-1021.

Smith, R.B., 1977: The steepening of hydrostatic mountain waves. *J. Atmos. Sci.*, **34**, 1634-1654.

Figure Captions

Fig. 1. The drag due to stationary linear mountain waves over North and South America and western Antarctica. The assumed surface wind is purely zonal at -7 m/s in the tropics and 13 m/s elsewhere. The assumed surface static stability and density are .01 s^{-1} and 1.0 kg/m^3, respectively. The arrow below the plot shows the scale for 2 Pa.

Fig. 2. The drag due to stationary linear mountain waves over Asia. The assumed surface wind is purely zonal at 10 m/s everywhere. The assumed surface static stability and density are as in Fig. 1. The scale for 2 Pa is shown by the arrow below the plot.

Fig. 3. Details of the scheme for separating the propagating part of the base flux from the nonpropagating (blocked or deflected) part. The hatched area is the cross-section presented to the blocked or deflected part of the flow.

Fig. 4. The distribution over Eurasia of the linear drag due to uniform westerlies, computed in 3 different ways: a) the analytic drag, b) the dimensional drag based on (filtered) topographic variance, and (c) the dimensional drag based on the integrated power laws proposed herein. Results for both dimensional formulas assume a drag coefficient $a_0 = 2$ and the power-law result uses $\mathrm{Fr}_0 = 1$, $\gamma = 0.8$ and $\varepsilon = 0.2$.

Fig. 5. The normalized propagating drag, $\langle D_p \rangle / D^*$, and total drag, $\langle D_p + D_{np} \rangle / D^*$, as a function of normalized maximum mountain height, $\mathrm{Fr}_{max} / \mathrm{Fr}_c$, for the two extreme cases $\mathrm{Fr}_{min} = 0$ and $\mathrm{Fr}_{min} = \mathrm{Fr}_{max}$ with $\gamma = 0.8$, $\beta = 0.5$ and $\varepsilon = 0.2$. The drag is normalized by the linear dimensional estimate D^* defined in Eq. 14. The nonpropagating part assumes $a_1 / (a_0 \mathrm{Fr}_c) = 9.0$.

Fig. 6. The distribution over North America of the normalized (a) propagating and (b) nonpropagating base flux according to the bulk dimensional analysis, with $\gamma = 0.8$, $\beta = 0.5$ and

$\varepsilon = 0.2$. The assumed large-scale surface wind is purely zonal at 8 m/s in the extratropics and -5 m/s in the tropics. The assumed static stability is $\bar{N} = 0.01\ \mathrm{s}^{-1}$.

Fig. 7. The normalized propagating drag $\langle D_p \rangle / D^*$ as a function of height for the two extreme cases $\mathrm{Fr}_{min} = 0$ and $\mathrm{Fr}_{min} = \mathrm{Fr}_{max}$ with $\gamma = 0.8$, $\beta = 0.5$, $\varepsilon = 0.2$ and $\mathrm{Fr}_{max} = 0.8\ \mathrm{Fr}_c$. The assumed wind profile (shown at right) has jets of 38 m/s and 58 m/s centered at heights of 9 km and 25 km, respectively. The static stability increases from $0.011\ \mathrm{s}^{-1}$ to $0.022\ \mathrm{s}^{-1}$ across $z = 11\ \mathrm{km}$ and the assumed density scale height is 9 km. The dashed curves show the local saturation drag. Momentum forcing, which is proportional to the derivative of the drag, is concentrated in layers above the two jets. Partial saturation and wavebreaking first occur near $z = 14\ \mathrm{km}$.

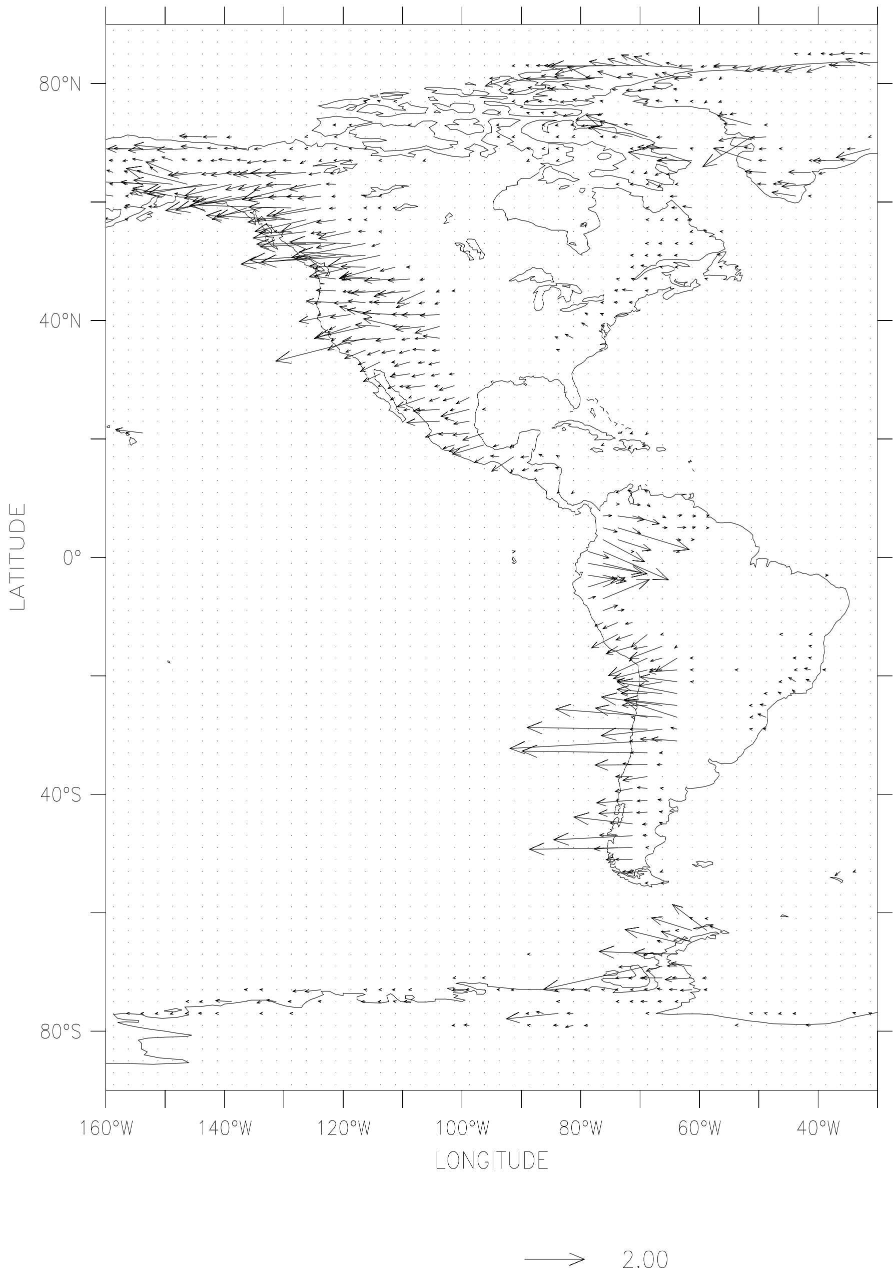

Fig 1. The drag due to stationary linear mountain waves over North and South America and western Antarctica. The assumed surface wind is purely zonal at -7 m/s in the tropics and 13 m/s elsewhere. The assumed surface static stability is .01 s^{-1}. The arrow below the plot shows the scale for 2 Pa.

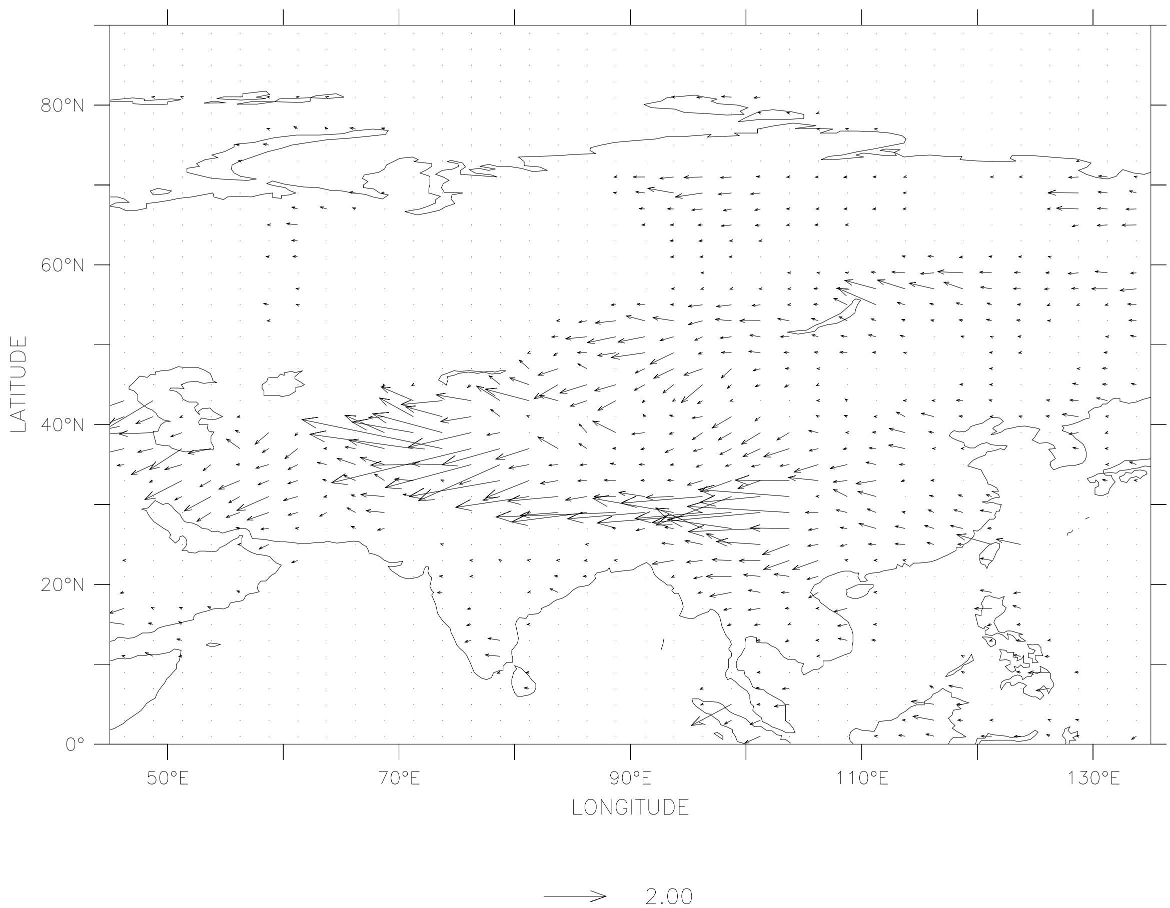

Fig 2. The drag due to stationary linear mountain waves over Asia. The assumed surface wind is purely zonal at 10 m/s everywhere. The assumed surface static stability is .01 s^{-1}. The scale for 2.0 Pa is shown by the arrow below the plot.

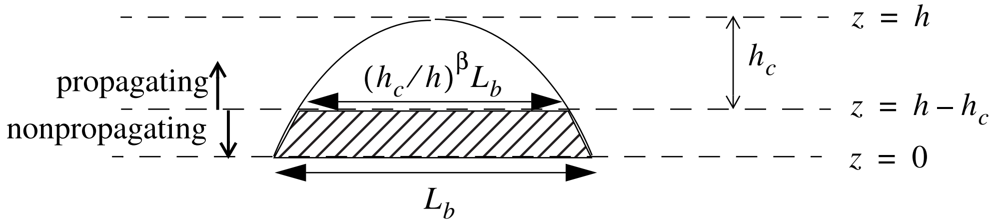

Fig. 3

Fig. 3. Details of the scheme for separating the propagating part of the base flux from the non-propagating (blocked or deflected) part. The hatched area is the cross-section presented to the blocked or deflected part of the flow.

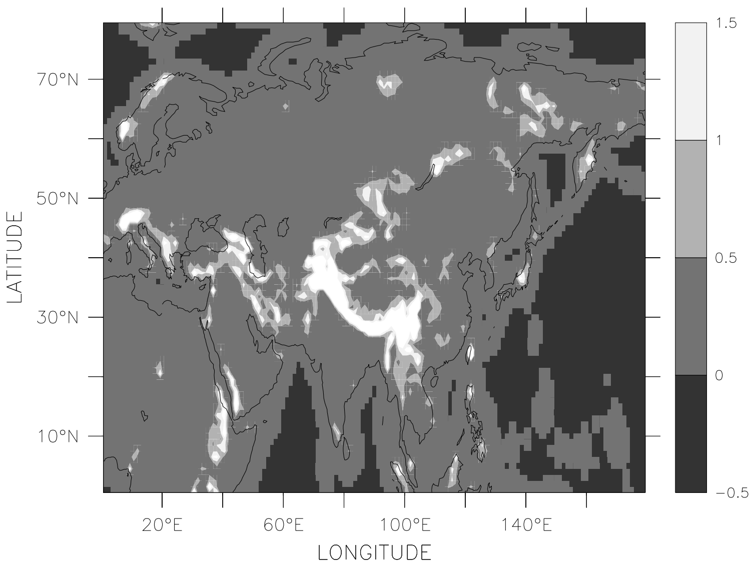

a) DRAG1

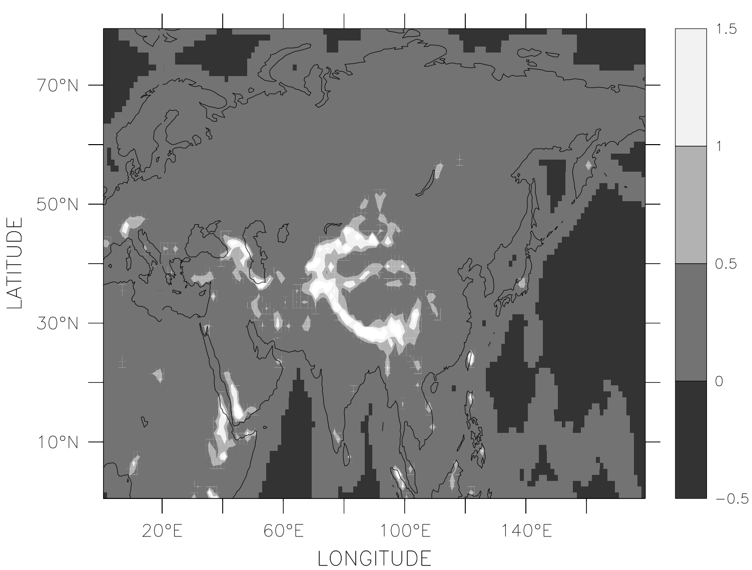

b) DRAG2

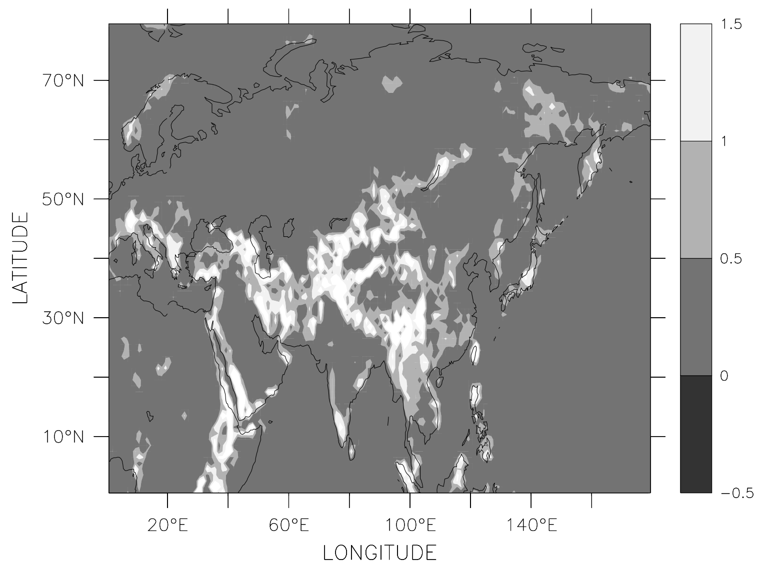

c) DRAG3

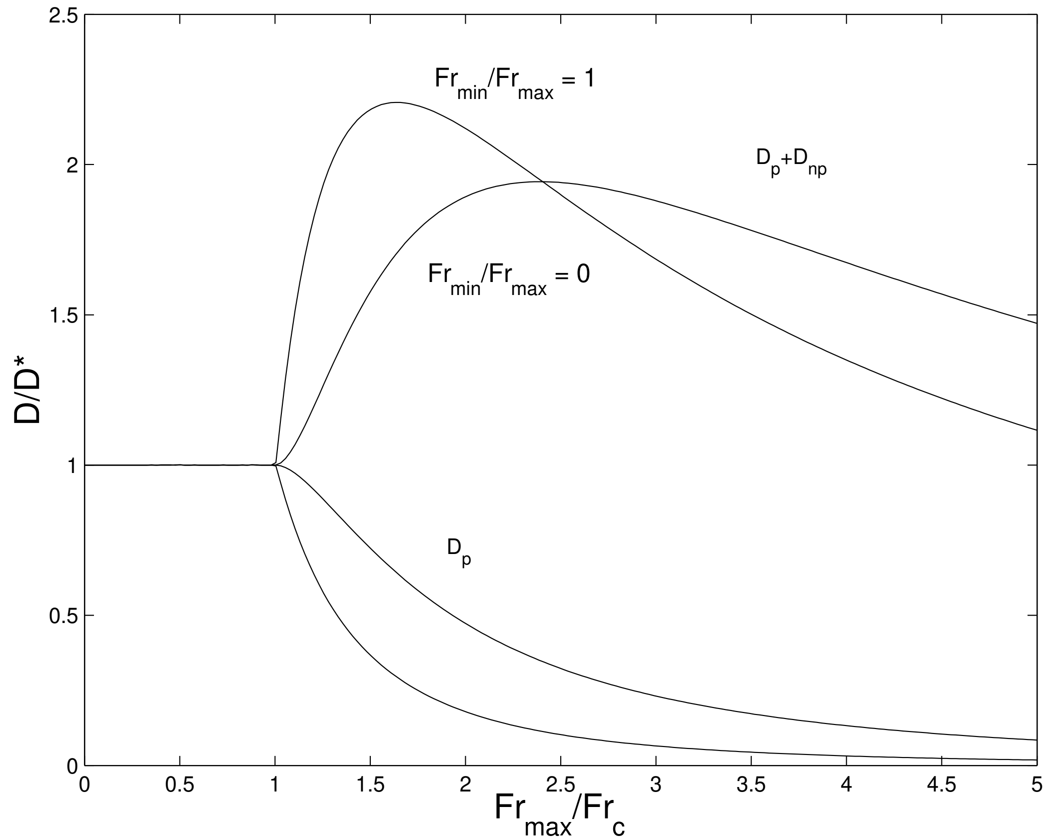

$Fr_{min}/Fr_{max} = 1$
D_p+D_{np}
$Fr_{min}/Fr_{max} = 0$
D_p
D/D*
Fr_{max}/Fr_c
2.5
2
1.5
1
0.5
0
0
0.5
1
1.5
2
2.5
3
3.5
4
4.5
5

(a)

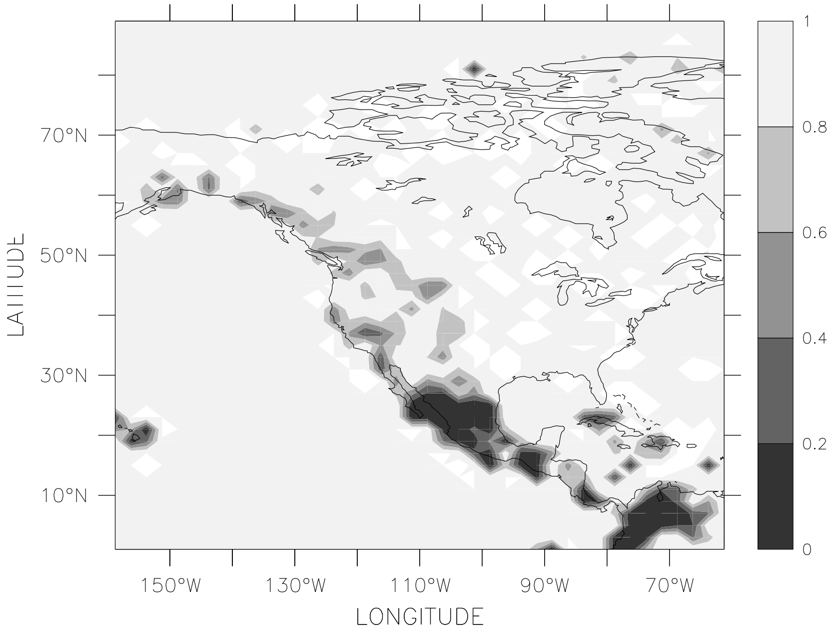

propagating fraction (none)

(b)

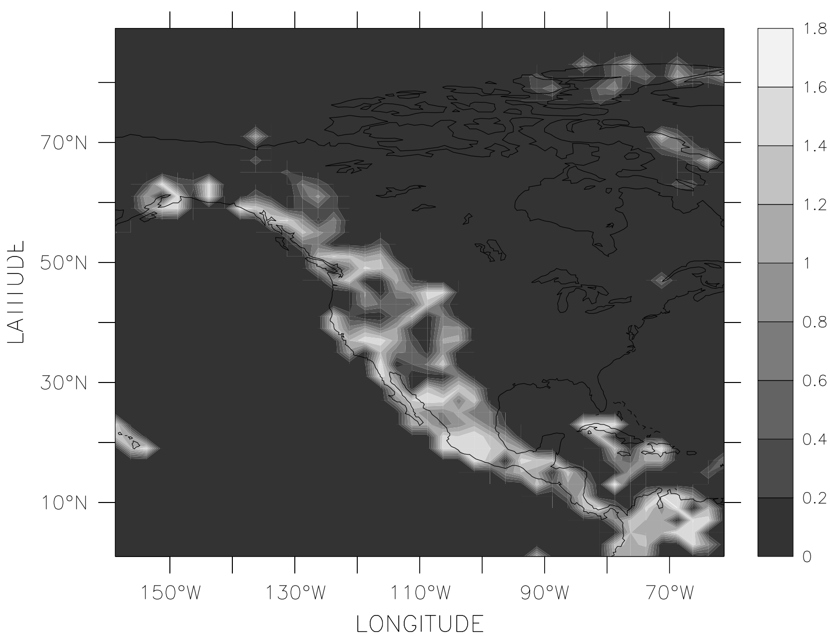

nonpropagating fraction (none)

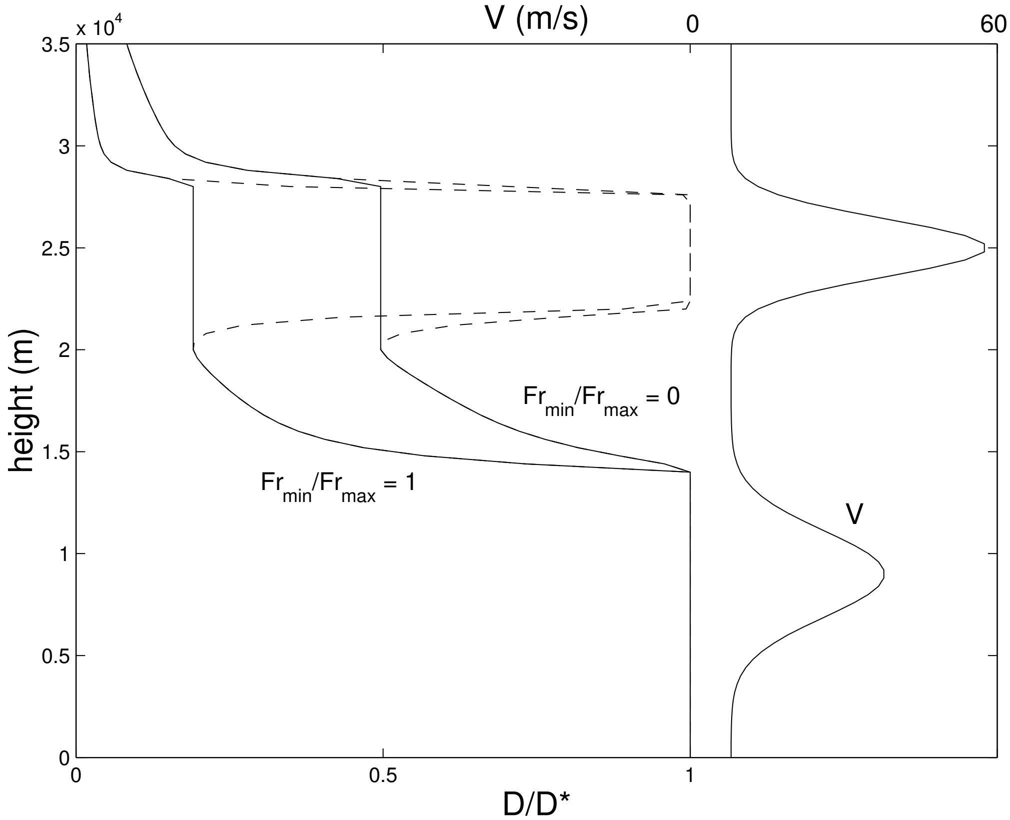

V (m/s)
0
60
x 10^4
3.5
3
2.5
2
1.5
1
0.5
0
height (m)
Fr_min/Fr_max = 0
Fr_min/Fr_max = 1
V
0
0.5
1
D/D*